Heliyon 8 (2022) e08683

Contents lists available at ScienceDirect

Heliyon

journal homepage: www.cell.com/heliyon

Research article

Computational and experimental characterizations of annealed Cu_2ZnSnS_4 thin films

Ahmad A. Ahmad [a], A.B. Migdadi [a], Ahmad M. Alsaad [a,*], I.A. Qattan [d], Qais M. Al-Bataineh [a], Ahmad Telfah [b,c]

[a] Department of Physical Sciences, Jordan University of Science & Technology, P.O. Box 3030, Irbid, 22110, Jordan
[b] Hamdi Mango Center for Scientific Research, (HMCSR), Jordan University, Amman, 11942, Jordan
[c] Leibniz Institut für Analytische Wissenschaften-ISAS-e.V., Bunsen-Kirchhoff-Straβe 11, 44139 Dortmund, Germany
[d] Department of Physics, Khalifa University of Science and Technology, P.O. Box 127788, Abu Dhabi, United Arab Emirates

ARTICLE INFO

Keywords:
Cu_2ZnSnS_4 (CZTS)
Thin films
Sol-gel
Optical properties
Structural properties
XRD
Kesterite
DFT
VASP

ABSTRACT

We report on the synthesis and characterization of Cu_2ZnSnS_4 (CZTS) thin films prepared at different annealing temperatures using the sol-gel method and deposited on glass substrates using the immersing method. The XRD analysis demonstrates that the films annealed at 450 °C exhibit the most stable tetrahedral kesterite structure. Computationally, the Vienna ab initio simulation package (VASP) has been implemented to calculate critical structural properties of as-prepared CZTS) thin films and compared with those extracted from the XRD patterns. An excellent agreement is obtained between the calculated and measured structural parameters. Optical measurement of key optical parameters of annealed CZTS thin films shows a drastic manipulation of all-optical properties compared to the as-prepared thin films. In particular, an optical band gap of 1.62 eV obtained for annealed CZTS thin films at 450 °C makes them eligible to be potential candidates for thin film-based high-efficiency solar cells. Calculations of elastic properties of annealed thin films reveal that crystallite size increases and microstrain decrease compared with those of as-prepared thin films. The sheet resistance of annealed CZTS thin films exhibits a significant decline as the annealing temperature is increased. The electrical properties of annealed CZTS thin films could match some conductors. Remarkably, at 450 °C annealing temperature, the sheet resistance decreases to 74 $\Omega.cm^{-1}$ indicating the possibility of using the annealed CZTS thin films for efficient and low cost solar cell applications.

1. Introduction

Solar energy is a plentiful, low-cost, and environmentally friendly source of electricity due to its significant characteristics such as its availability, developed technology, robustness [1]. Silicon (Si) solar cells presently control the photovoltaic sales (>80%). However, its low absorption coefficient hindered the fabrication of high efficiency of Si-based solar cells. Compounds such as Cadmium Telluride (CdTe), Copper Indium Gallium Selenide (CIGS), and Copper Zinc Tin Sulfide (CZTS)) that exhibit high absorption coefficient could be potential alternatives to silicon for the manufacturing of high-efficient multifunctional solar cells. The photovoltaic properties of inorganic thin-film solar cells have attracted much attention owing to their extraordinary properties and high efficiency. For instance, CIGSe-based solar cells exhibit 20.3% efficiency straightforwardly [2]. Nevertheless, a scaled industrial production of CIGSe solar cells appears to be held up by the scarcity of In and Ga components in the earth's crust. Promising alternatives have been proposed. The quaternary compound Cu_2ZnSnS_4 (CZTS) has attracted substantial consideration as a promising contender because it is entirely composed of earth-abundant elements. It exhibits a crystal structure that resembles that of CIGS [3]. Several successful attempts to fabricate CZTS thin-film solar cells have been reported [4, 5].

CZTS thin-film solar cells are recently produced on an industrial scale. Their optical band gap energy and absorption coefficient are estimated to be about 1.5 eV and 10^4 cm^{-1}, respectively [6, 7]. It exhibits a p-type conductivity in the kesterite structure [8]. Subsequently, crucial improvements have been achieved in manufacturing CZTS thin film-based solar cells [9]. Regardless of their anticipated ~32.2% power transformation efficiency [10], the maximum recorded efficiency of CZTS-Se thin-film solar cells is as tiny as 12.6% [9]. The need for elaborated work

* Corresponding author.
E-mail addresses: alsaad11@just.edu.jo, amalsaad@unomaha.edu (A.M. Alsaad).

https://doi.org/10.1016/j.heliyon.2021.e08683
Received 12 July 2021; Received in revised form 17 September 2021; Accepted 23 December 2021

to develop the synthesis, characterization, and fabrication of CZTS solar cells is necessary. The challenge is to increase the energy conversion efficiency to an optimum value that permits the production of solar cells at a commercial scale.

The real challenge for the solar cells sector is to design and fabricate cells of specific features such as that high efficiency, low cost; their components are abundant on the earth crust, friendly to the environment, and nontoxic [11]. Based on our understanding, the reported experimental efficiency of CZTS solar cells is still low compared with theoretically calculated values [12]. Up to date, the highest reported experimental efficiency of pure CZTS solar cells fabricated by the co-sputtering method is 11% [13]. In addition, CZTSSe thin film solar cells fabricated using the spin coating technique based on the hydrazine solution processing exhibit efficiency of 12.6% [14]. CZTS thin-film solar cells with an efficiency of 8.4% using a vacuum-based thermal evaporation process have been reported last decade [15]. CZTSSe solar cells with an efficiency of 9.2% using the co-evaporation method have also been reported [16]. Consequently, further elaboration is needed to elucidate the electronic, structural, and optical properties of CZTS solar cells and achieve the highest possible efficiency. The theoretical efficiency of more than 30% has been predicted using photon balance calculations [12]. It is worth mentioning that the highest efficiency of thin-film solar cells been reported is 20% utilizing expensive and non-abundant materials such as Indium (In), Gallium (Ga), and Tellurium (Te) and some toxic materials such as Cadmium (Cd) [17].

The CZTS crystallize into two different types of crystal structures. Mainly, stannite (ST) and kesterite (KS). Both belong to the tetragonal system. The difference is in the atomic arrangements of Zn and Cu and the slight difference in the binding energy of ~3 MeV/atom. The kesterite is the most stable structure of CZTS. The thermodynamical properties of CZTS thin films in the kesterite phase enable them to be the most appropriate for solar cell applications as compared with the corresponding properties in the stannite structure [18, 19]. A pioneering study revealed that annealing temperature plays an essential role in improving crystal structure and decreasing structural defects of CZTS thin films [20]. Accurate calculation of the elastic parameters of CZTS thin film solar cells is crucial for the fabrication of highly efficient solar cells. The solar material is being subjected to stress and strain during production and utilization. Therefore, determining the stiffness of solar cells by calculating Young's modulus is extremely important [21, 22]. Moreover, precise determination of the elastic properties of CZTS strongly influences the quality of intergrain and heterostructure interfaces during the fabrication process of thin film solar cells [22].

Synthesis of CZTS thin films was performed using different techniques such as thermal evaporation [23], sputtering [24], electrodeposition [25], spray pyrolysis [26], Pulsed Laser Deposition [27], sol-gel, microwave, hydrothermal, solvothermal [19], etc. However, chemical techniques are considered more straightforward than physical techniques in cost, equipment, and materials. Nevertheless, they are not devoid of disadvantages like non-uniform coating and cracks [19].

The main objective of this work is geared towards investigating the effect of annealing temperature on the structural, physical, and chemical properties of CZTS thin films. In particular, obtaining the optimum annealing temperature is crucial in achieving optimized structures of CZTS thin films that exhibit extraordinary structural, physical, and chemical properties. To elucidate a better understanding of the experimental findings, we investigate the optimized structural parameters of CZTS using the total energy minimization approach employed in the Vienna ab initio simulation package (VASP) [28]. An excellent agreement between the experimental and the theoretical structural lattice parameters is revealed in this work.

2. Experimental procedure

2.1. Experimental procedure

The fused silica glass substrates are washed with methanol and acetone, rinsed with deionized water in an ultra-sonication bath to remove organic impurities. The substrates are then dried out using an N_2 jet torrent. The CZTS solutions are prepared by the sol-gel method. A 2.39 g of copper acetate dehydrate, 1.54 g of zinc acetate dihydrate, 1.14 g of tin chloride, and 1.83 g of thiourea are dissolved in 50 ml of 2-methoxyethanol (solvent). After completely dissolving the materials, a few droplets of monoethanolamine (MEA) (stabilizer) were added to the mixture at about 60 °C. The 1:1 M ratio of monoethanolamine to zinc acetate dihydrate is chosen. The mixture was stirred for 3 h at 90 °C. It then left to cool at room temperature for one day before use.

CZTS thin films were deposited by immersing the pre-cleaned substrates into CZTS solution for 2 h to produce a one-layer thin film at room temperature. The samples were treated with post drying in an oven at 85 °C for 30 min to evaporate the solvent and organic residues. Finally, CZTS films were annealed in air at various temperatures for a 1-h duration.

Powder XRD (Malvern Panalytical Ltd, Malvern, UK) (220–230 VAC 50/60 Hz 40 A) using Cu-Kα_1 ray with a wavelength of 0.1540598 nm at room temperature is utilized to elucidate the crystallinity of CZTS thin films. The angle of incidence is varied from 10^o to 70^o. The angles are varied in steps of 0.02^o with an energy resolution of 20%. The angular resolution of 0.026° FWHM on LaB_6.Angular reproducibility of <0.0002° is adjustable. The maximum angular velocity of 15 deg./s is maintained. The chemical properties were analyzed using Fourier-transform infrared spectroscopy (Bruker VERTEX 80/80v Vacuum FTIR Spectrometers). The scanning electron microscope (SEM, Quanta FEG 450) was used to study the surface morphology of thin films. The optical transmittance and reflectance spectra are measured using a UV–Vis spectrophotometer (U–3900H at room temperature. Finally, the electrical properties were determined by (Keithley 2450 SourceMeter).

2.2. Method of calculation

All calculations are performed within the framework of the density functional theory (DFT) [29]. The exchange-correlation term of the pseudopotential is treated using generalized gradient approximations (GGA) [30]. The electron-ion pseudopotentials are obtained by implementing the projector augmented wave (PAW) scheme [31, 32, 33] embedded in the Vienna *ab-initio* simulation package (VASP) [34, 35, 36]. A mesh of dimensions $4 \times 4 \times 2$ is used to describe the Brillouin zone in the reciprocal space for the geometry optimizations, followed by monitoring Hellmann-Feynman forces and total energy minimization of the unit cell. The energy cut-off is set to 520 eV [37, 38]. The atomic positions in the unit cell are minimized to yield optimized structures. The optimized lattice parameters obtained are in good agreement with the previous experimental and theoretical findings. The same computational procedure is utilized to compute the electronic and elastic properties using thin films based solar cells.

3. Results and discussion

3.1. Structural and electronic properties

As demonstrated in Figure 1, CZTS crystallizes in a tetragonal body-centered kesterite structure. We examined the structural properties of CZTS thin films computationally and experimentally. Mainly, we applied DFT-based simulations to obtain the optimized lattice parameters of

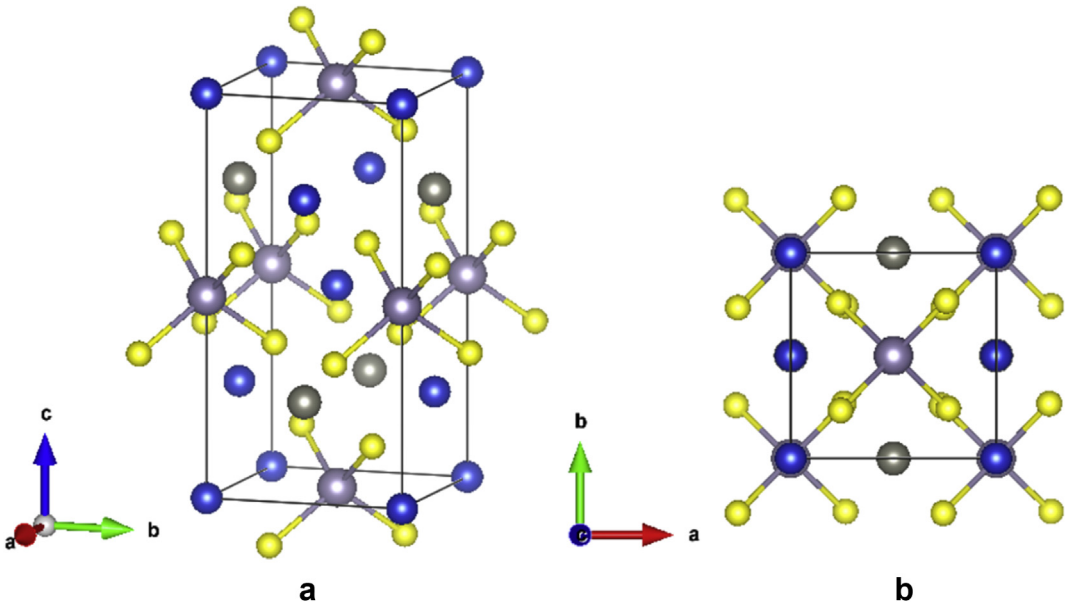

Figure 1. Schematics of (a) 3-D CZTS crystal construction and (b) 2-D CZTS crystal assembly.

CZTS. In addition, XRD measurements are analyzed to elucidate the structural properties of the CZTSthin films. Computationally, structural properties are characterized by minimizing the total energy of the unit cell (i.e., as small as 10^{-8} eV) and the Hellmann–Feynman forces to be approximately 0.002 eV/Å at convergence. Minimization of total energy and Hellmann–Feynman forces ensure obtaining highly accurate lattice parameters of the CZTS system. Furthermore, optimization of lattice parameters is crucial for the accurate calculation of the electronic and optical properties of CZTS thin films. The equilibrium in-plane and out-plane lattice parameters a, b, and c of CZTS thin film are depicted in (Figure 1(a)). We found $a = b = 6.556$ Å and $c = 13.085$Å.

Figure 2 shows XRD patterns of CZTS thin films at different annealing temperatures (as prepared, annealed at 250 °C, 350 °C, and 450 °C) exposed for a 1-h duration. The angle of incidence was varied from 20° to 70°. The XRD results indicate that the as-prepared film is amorphous, with no diffraction peaks are noticed [39]. The film acquires the amorphous structural form due to the fact that the constituent atoms and molecules are accumulated at random sites in the lattice due to the lack of enough heat-energy needed to activate their vibrational motion in order to rest at sites of minimum energies. XRD pattern peaks of CZTS thin films

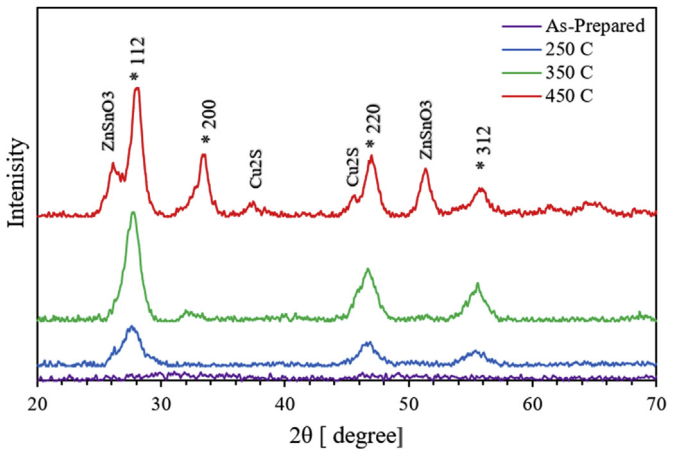

Figure 2. The XRD patterns of CZTS thin films at different annealing temperatures.

annealed at 250° and 350° are similar but with different intensities. Three peaks at 2θ = 27.5°,46.6°, and 55.4° were appeared corresponding to (112), (220) and (312) crystallographic planes, respectively. For the Cu_2ZnSnS_4 film annealed at 450°, four major peaks appeared at 2θ = 27.5°,33.5°,46.6° and 55.4° corresponding to (112), (200), (220), and (312) crystallographic planes, respectively in good agreement with previous studies [24, 40, 41]. It has been reported that the crystal structure of the CZTS thin films is kesterite belongs to the tetragonal system [7, 40, 41, 42]. Moreover, there are secondary phases that appeared for the sample annealed at 450 C°; the two peaks at $2\theta =$ 26.6° and 51.5° belong to $ZnSnO_3$ [40]. The other two small peaks at $2\theta =$ 37.5° and 45.6° belong to Cu_2S [43]. These two secondary phases will affect the crystal structure and lattice parameters hence the optical bandgap energy. The influence of secondary phases of $ZnSnO_3$ and Cu2S in CZTS absorber material can be understood by calculating the band offsets at the CTS/CZTS/ZnS multilayer heterojunction interfaces based on DFT band structure calculations. Since ZnS has a larger band gap than that of CZTS, the ZnS phase in CZTS is predicted to be resistive barriers for carriers. The band gap of CTS is located within the band gap of CZTS. Therefore, the CTS phase acts as a recombination site in CZTS and thus increase the band gap more than expected.

The peak intensities increased by increasing the annealing temperature from 250° to 450°, indicating a higher degree of crystallinity [17, 39]. The (a and b) lattice constants of the CZTS thin films are evaluated by Eq. (1).

$$\frac{1}{d^2} = \frac{h^2 + k^2}{a^2} + \frac{l^2}{c^2} \tag{1}$$

where: d is the interplanar spacing that can be determined using Bragg's law ($\lambda = 2d_{hkl} \sin \theta_{hkl}$). The lattice constants of CZTS thin film annealed at 450 °C are found to be $a = b = 6.941$ Å and $c = 13.337$Å, in good agreement with DFT-based calculations. It is worth mentioning that the standard values of the CZTS are $a = b = 5.45$ Å, $c = 10.9$ Å. Thus, the increase in the obtained experimental values of the lattice parameters may be attributed to the formation of the secondary phases such as, $ZnSnO_3$ and Cu_2S.

The average crystallite size (D) and the microstrain (ε) of CZTS thin films at different annealing temperate are calculated using Debye Scherrer's formula as represented in Eqs. (2) and (3) [41, 44].

$$D = \frac{\lambda K}{\beta \cos\theta} \quad (2)$$

$$\varepsilon = \frac{\beta \cot\theta}{4} \quad (3)$$

where k is constant equals 0.94, β is the full width at half maximum (FWHM) measured in radians, λ is the wavelength of the X-ray (λ = 0.154184 nm), and θ is Bragg's angle (peak position). The D and ε parameters are plotted as a function of annealing temperature, as shown in Figure 3. The D parameter of CZTS thin films at 250 °C 350 °C and 450 °C annealing temperatures is found to be 4.8 nm, 5.5 nm, and 8.3 nm, respectively. As can be seen, D increases as annealing temperature increases. On the other hand, ε significantly decreases as the annealing temperature is increased. This indicates that annealing temperature greatly influences controlling D and the related fundamental crystal properties, according to previously reported results [39, 45]. The structural distortions and defects are reduced, as indicated by the decrease in the microstrain and the enhancement of the crystallite size. The increase in the crystallite size leads to the reduction of the microstrain [46, 47]. Consequently, the optical band gap is decreased, and the absorption is increased as a result of the reduction of the microstrain [48]. Since the band gap energy and optical absorption are crucial for enhancing the photovoltaic performance of solar cells, the decrease of the microstrain and the increase of the crystallite size of CZTS thin films are the critical parameters of the enhanced photovoltaic performance of CZTS solar cells [49].

To further elucidate the effect of annealing temperature on the crystal properties, the Crystallite density (N) and the dislocations density (δ) are calculated using $N = t/D^3$ and $\delta = 1/D^2$, respectively, where D is the crystallite size, t is the film thickness. The N and δ parameters are plotted as a function of annealing temperature, as shown in Figure 4. Clearly, δ decreases from 4.3 * 10^{12} lines/cm^2 to 1.6 * 10^{12} lines/cm^2 as annealing temperature increases from 250 °C to 450 °C. This can be attributed to the relaxation and enhanced crystallinity of thin films at high annealing temperatures. However, the N parameter decreases as the annealing temperature increases. This indicates that N and δ exhibit a reverse behavior as annealing temperature is increased.

The electronic properties of CZTS are obtained by implementing self-consistent electronic ab initio simulations. In particular, the electronic density of states (DOS), the partial density of states (PDOS), and the electronic band structure are calculated self consistently [50]. Figure 5(b) shows DOS and PDOS of CZTS thin film using GGA approximation. Figure 5(c) depicts the electronic band structure of the CZTS thin films. Interestingly, CZTS thin films exhibit a direct bandgap at Γ point consistent with that of bulk CZTS. As anticipated, the calculated optical band gap is underestimated largely compared with the experimental value [51, 52, 53]. The theoretical optical direct bandgap energy of CZTS thin films is estimated to be 1.33 eV.

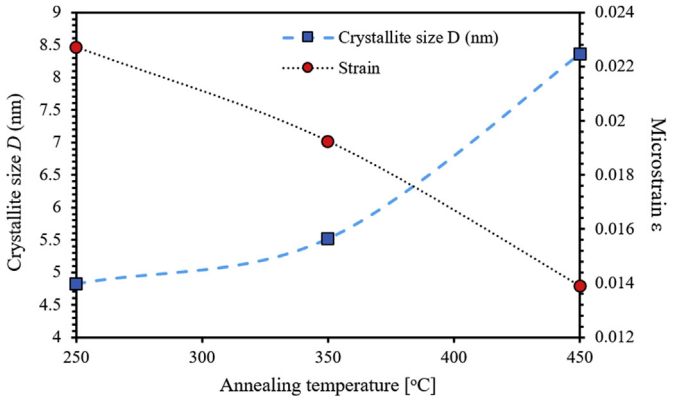

Figure 3. The crystallite size D and the microstrain ε of CZTS thin films at different annealing temperatures.

3.2. Surface morphology analysis

The surface morphology of CZTS thin films was analyzed using a scanning electron microscope (SEM). Figure 6 (a-b) shows the SEM micrographs of surface morphologies of CZTS films (as prepared, annealed at 250 °C, and 450 °C). As shown in Figure 6a, the as-prepared CZTS thin film is amorphous and exhibits a polished smooth surface. The CZTS films annealed at 250 °C and 450 °C exhibit spherical particles that become more apparent and crystallized at 450 °C, as shown in Figures 6b and 6c. The results obtained from SEM micrographs are consistent with structural analysis based on the XRD patterns. The results obtained from the SEM micrographs indicate that increasing the annealing temperature above 450 °C could result in high-quality large-grained CZTS thin films and thus films exhibiting extraordinary optical and electrical properties.

3.3. Chemical properties

The FTIR spectrum of CZTS thin films is measured at different annealing temperatures in the (4000–500) cm^{-1} wavenumber range and presented in Figure 7. The extended peak of as-prepared CZTS thin films between 3700 and 2500 cm^{-1} is due to sulfur-rich composition. A series of peaks ranging from 900 to 1600 cm^{-1} are attributed to the stretching and bending of oxygen vibrations. The peaks reveal the Zn–S bond and S–H bond stretching at 575 and 460 cm^{-1}, respectively [54]. Peak depicted at 1613 cm^{-1} could be assigned as symmetrical stretching of C=S bond. The peak associated with the Kesterite sulfur-rich composition is located at 1062 cm^{-1}. Characteristic absorptions at 2070 and 2330 cm^{-1} are fingerprints of thiol groups [55]. The peaks due to –OH, –CO, –SH, and CO_2 are recognized owing to the hygroscopicity of CZTS thin films and the surface adsorption of CO_2 [56].

3.4. Optical properties

Figures 8 and 9 show the transmittance (T%) and reflectance (R%) spectra of CZTS thin films treated with various annealing temperatures as a function of wavelength in the range of 250–800 nm. It can be noticed that a significant increase in the transmittance values of the as-prepared CZTS thin film from about 0% up to 85%as the wavelength increases from 300 nm to 500 nm. It then attains an almost flat constant value as the wavelength is increased to 800 nm. The transmittance decreases for CZTS films annealed at 250 °C, 350 °C, and 450 °C. Upon annealing, the band edge is shifted into the red region leading to an optical bandgap decrease. This could be attributed to increased grain size, structural homogeneity, and crystallinity [51, 57].

Moreover, the reflectance spectra of as-prepared CZTS thin films decline from 12.5% to 4.7%as the wavelength is increased from 250 nm to 700 nm. Apparently, the reflectance values decrease continuously for CZTS films annealed at 250 °C, 350 °C, and 450 °C. The increase of reflectance values between 700-800 nm can be attributed to the high reflectance of NIR-IR from the surface of glass substrates. There is an apparent decrease in transmittance and reflectance spectra of CZTS thin films by increasing the annealing temperature indicating a loss of light due to the high absorption.

Transmittance (T%) and reflectance (R%) spectra of CZTS thin films are utilized to calculate other critical optical properties like absorption coefficient (α), extinction coefficient (k), optical band gap energy (E_g), and refractive index (n). This is necessary to reveal the effect of annealing temperature on the optical properties of thin films. The absorption coefficient (α) was calculated as $\alpha = (1/d)ln(1/T)$, where T is the transmission values and d is the thickness of the thin film (500 nm) [44, 58]. Figure 10 shows the absorption coefficient (α) of various annealed CZTS thin films as a function of wavelength. The absorption coefficient of CZTS films increases drastically as the annealing temperature increases compared to that of the as-prepared thin films. For $\lambda < 350$ nm, α attains its highest values. However, for $\lambda > 350$nm, α is vanishingly small. The variation in absorption coefficient with respect to annealing temperature

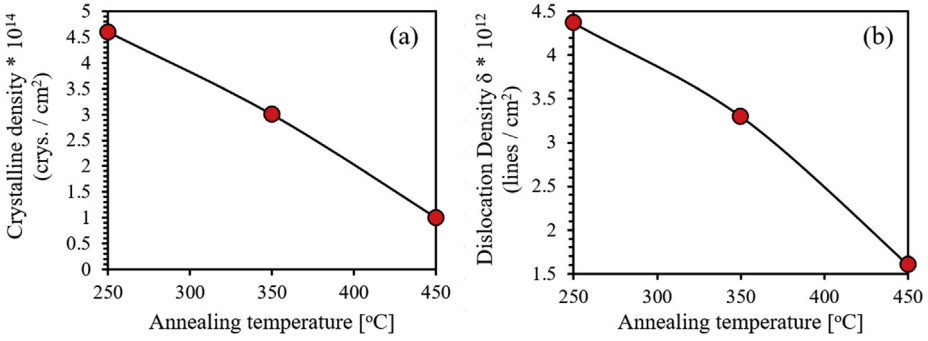

Figure 4. (a) The Crystallite density (N) and (b) the dislocations density (δ) of CZTS thin films as a function of annealing temperature.

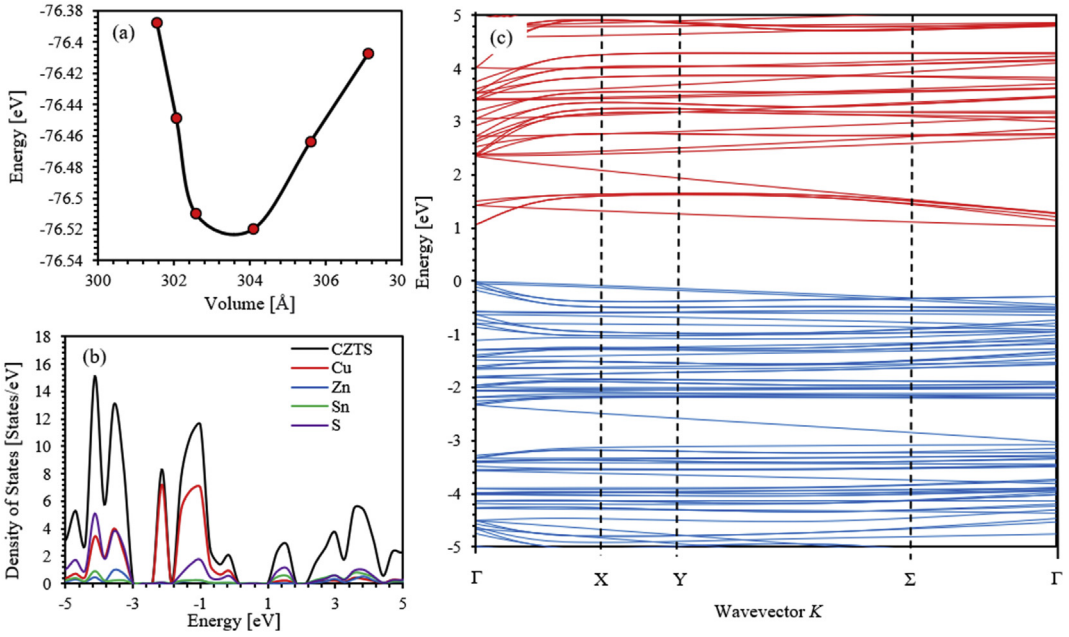

Figure 5. (a) The total energy versus the volume of the unit cell, (b) Calculated electronic band structure, and (c) Total DOS and PDOS of CZTS thin films.

may be attributed to the increase of the crystalline size and crystallinity as the annealing temperature increases, consistent with the interpretation of the XRD patterns [59, 60, 61].

Another essential optical parameter is the extinction coefficient (k) which can be calculated as $k = \alpha\lambda/4\pi$, where λ is the wavelength and α is the absorption coefficient [62]. It is considered as a measure of light energy loss by absorption and scattering per unit volume. Figure 11 shows the behavior of the extinction coefficient (k) of annealed CZTS thin films as a function of the wavelength. The extinction coefficient of CZTS films increases as the annealing temperature increases compared to that of as-prepared thin films. The highest extinction coefficient values are attained for $\lambda < 350$ nm, indicating the highest absorption in this spectral region. For $\lambda > 350$ nm, k decreases as λ increases demonstrating that absorption and scattering gradually diminish.

The optical band gap energy (E_g) of all CZTS samples is estimated using Tauc's plot method. It gives the relationship between the photon energy ($h\upsilon$), the absorption coefficient (α), and the band gap energy. The relationship is given by the following formula (equation 4) [63, 64].

$$(\alpha h\upsilon)^{\frac{1}{n}} = A(h\upsilon - E_g) \tag{4}$$

where A is the constant known as band tailing, and n is the power factor of the transition depending on the nature of thin films (crystal or amorphous) equal to 1/2 for direct transition and 2 for indirect transition. The linear relationship between the $(\alpha h\upsilon)^2$ and the photon energy ($h\upsilon$) indicates that the thin film allows the direct transition, and the CZTS thin films exhibit a direct band gap energy [11]. Figure 12 shows the band gap energy (E_g) of annealed CZTS thin films using Tauc plots. The significant reduction of E_g reveals the effect of annealing temperature. It decreases from 2.62 eV for as-prepared CZTS thin film to 2.34 eV, 1.93 eV, and 1.62 eV, as the films are annealed at 250 °C, 350 °C, and 450 °C, respectively. This reduction in the optical band gap energy of annealed CZTS thin films may be attributed to the simultaneous increase in the crystallite size and decrease of the number of defects of the CZTS thin films as the annealing temperature is increased as reported in literature [59, 65]. The E_g value of 1.5 eV associated with a high absorption coefficient of more than 1×10^4 cm^{-1} is fair enough for the efficient operation of thin film-based solar cells. Evidently, annealed CZTS thin films exhibit excellent optical properties and can be appropriately developed and used for solar cells [7, 24]. Moreover, the minimum obtained value of E_g is 1.62 eV that is higher than the optimum value. This could be attribute to the existence of the $ZnSnO_3$ and Cu_2S secondary phases in the structure CZTS thin films.

Accurate calculation of the refractive index n is crucial for implementing thin films in optical devices [66]. The n parameter of CZTS thin films can be calculated as $n = (1 + R/1-R) + \sqrt{(4R/(1-R^2) - k^2}$. Figure 13 shows n spectraofas-prepared and annealed CZTS thin films. It

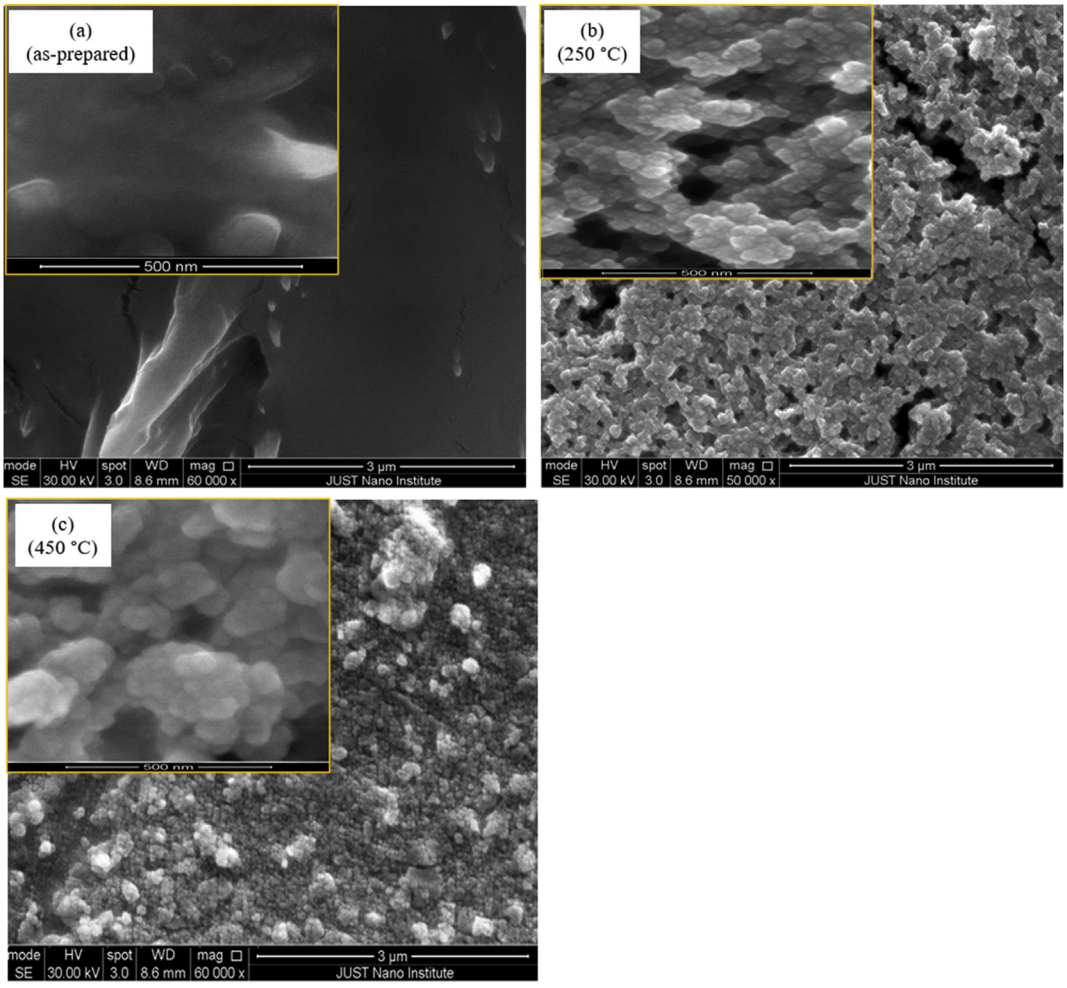

Figure 6. The SEM micrographs of the surface of CZTS films a) as-prepared; b) annealed at 250 °C; c) annealed at 450 °C.

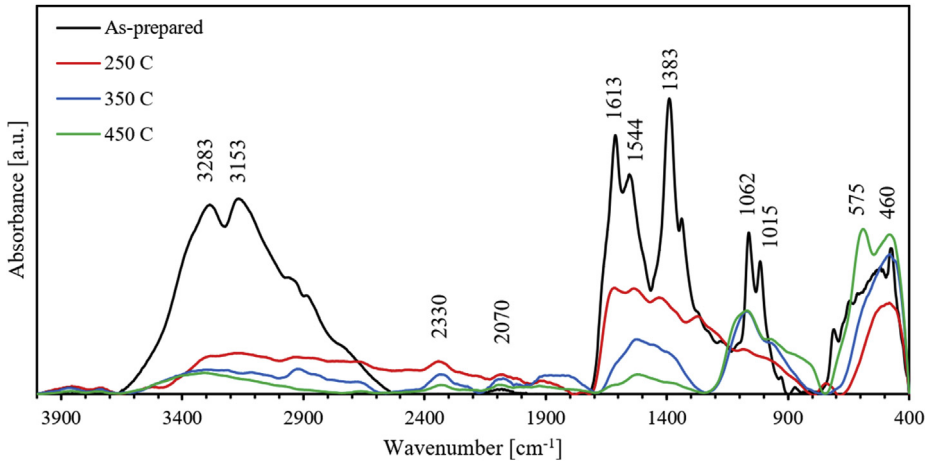

Figure 7. The FTIR spectra of CZTS thin films at different annealing temperatures.

is found that as-prepared CZTS thin film exhibits $n = 1.58$ at $\lambda = 550$ nm. Remarkably, CZTS thin films annealed at 250 °C, 350 °C, and 450 °C exhibits $n = 1.4$, 1.37, and 1.36, respectively. The significant reduction of n with annealing temperature is critical for applying CZTS thin films in designing a new generation of solar cells.

3.5. Elastic properties

The elastic parameters determine the stiffness response of material when subject to an external force [22]. The stiffness determines the response of a crystal to an externally applied strain or stress and provides

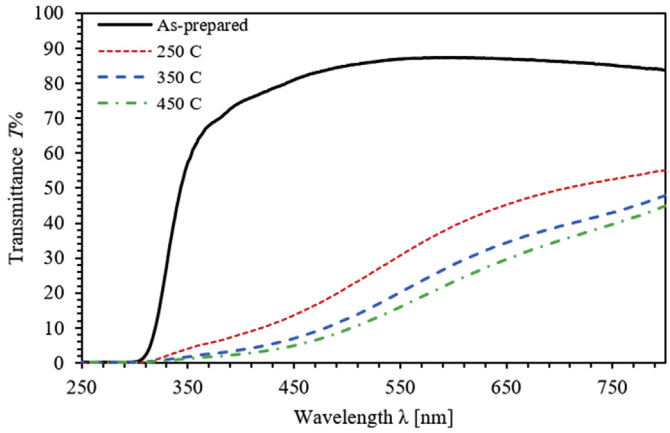

Figure 8. The transmittance spectra of CZTS thin films at different annealing temperatures.

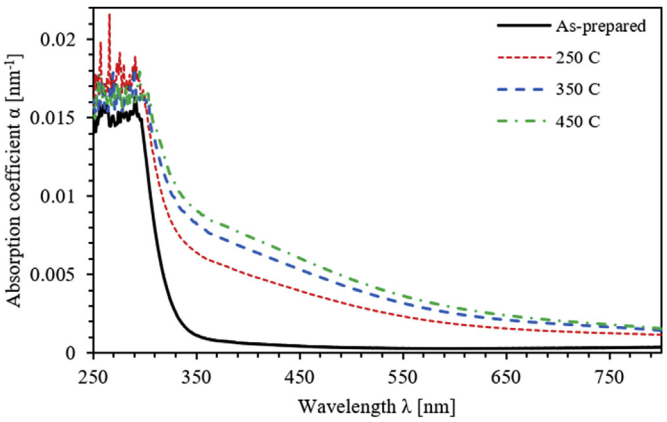

Figure 10. The absorption coefficient (α) of CZTS thin films at different annealing temperatures.

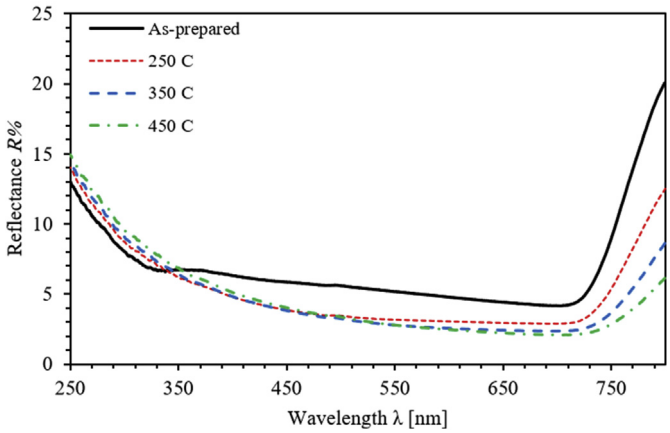

Figure 9. The Reflectance spectra of CZTS thin films at different annealing temperatures.

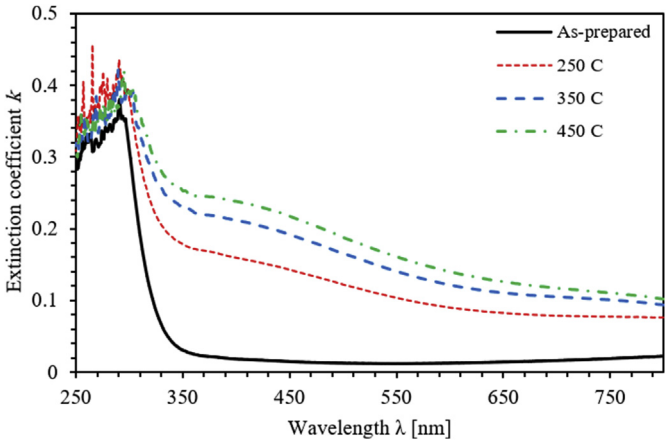

Figure 11. The extinction coefficient (*k*) of CZTS thin films at different annealing temperatures.

information about the bonding characteristics and the structural and mechanical stability [21]. To obtain a deeper insight into the elastic properties of CZTS thin films, we implement generalized gradient approximation (GGA) to calculate Bulk modulus (K), Shear modulus (G), Young's modulus (E), and Poisson's ratio (ν) utilizing the components of elastic moduli (C_{ij}) matrix [67]. GGA is trustfully approximation to the exchange-correlation part of the pseudopotential in the density functional theory (DFT) for ab initio calculation of the total energy. Young's modulus expresses the level of stiffness where the greater value of Young's modulus indicates that the material has more hardness. In contrast, the bulk and shear modulus expresses fracture and plastic distortion resistance, respectively [21, 68, 69].

The results are presented in Table 1. To elucidate the mechanical efficiency of the films, we perform mechanical stability tests. The elastic constants of the CZTS satisfy the $C_{11} \approx C_{33}$ stability condition. It indicates that bonding strength along [100] [010], and [001] directions are the same. Furthermore, $C_{11} + C_{12}$ is larger than C_{33} indicating that the elastic modulus value is higher in the (001) plane than along the *c*-axis. In addition, the fact that $C_{66} \approx C_{44}$ indicates that the [100] (001)-shear is comparable to the [100] (010)-shear for the two phases. The bulk modulus of CZTS is obtained to be 67.74 GPa. The Poisson's ratio (ν) provides information about the stability degree of the crystal against shear, and it usually ranges from -1 to 0.5 [68,69]. The ν is estimated to be about 0.3, indicating that CZTS has good plasticity. The ratio, K/G, is proposed by Pugh [70] to predict the brittle or ductile behaviour of thin films. According to the criterion, a high K/G value indicates a tendency for ductility. If $K/G > 1.75$, then ductile behavior exists. Otherwise, the material exhibits a brittle nature. The K/G ratio of CZTS is found to be 2.32, indicating that the CZTS is more prone to ductility.

3.6. Electrical properties

The as-prepared CZTS thin films do not need to be treated at high temperatures for specific applications. This can be understood in terms of piezoelectric applications such as piezoelectric actuators, transducers, buzzers, and ignitors. The harvesting of energy is possible by using piezoelectric as prepared CZTS thin films to convert stress or strain into electrical energy. Having calculated the main elastic coefficients (C_{ij}) as reported in Table 1, The piezoelectric coefficients e_{ij} and converse piezoelectric coefficients d_{ij} tensor matrices can straightforwardly be calculated. The calculated piezoelectric tensor matrices are crucial for understanding the electromechanical coupling of the CZTS thin films. The piezo current and voltage are critical parameters for the functioning of piezoelectric transducers. It is necessary to plot the I–V characteristics of CZTS thin films to elucidate their electrical behavior.

The I–V characteristics are plotted in Figure 14 (a) to reveal the electrical properties of CZTS thin films. The applied voltage is in the (−20 to 20 mV) range. A linear relationship is obtained for as-prepared and annealed thin film samples. Figure 14 (b) shows the sheet resistance of CZTS thin films extracted from the slope of the I–V characteristics. A significant decline of the sheet resistance is observed as the annealing temperature increases. Remarkably, a decrease from 625 $\Omega.cm^{-1}$ for as-prepared CZTS thin film to only 74 $\Omega.cm^{-1}$ for CZTS thin film annealed at 450 °C.

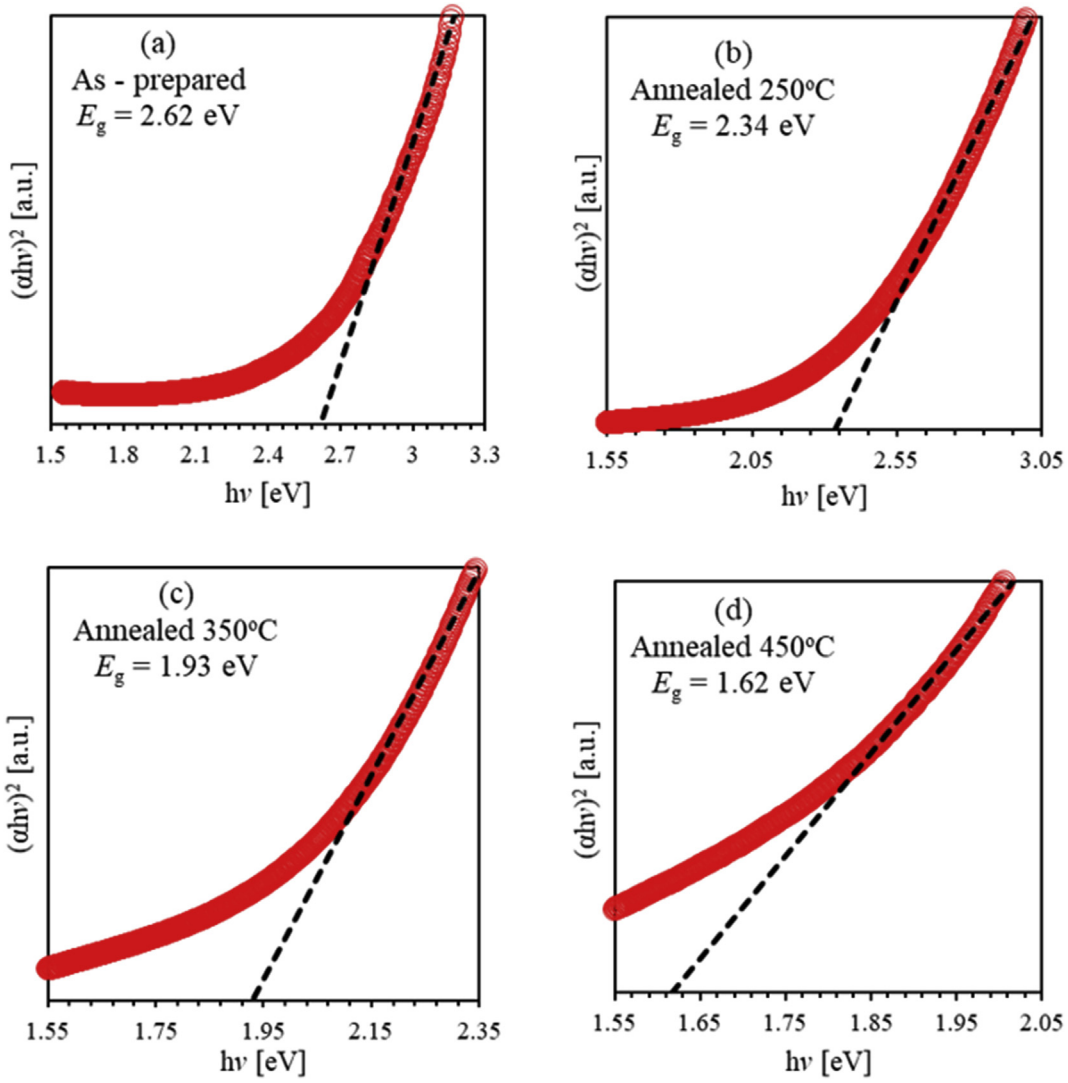

Figure 12. The optical bandgap energy E_g of CZTS thin films at different annealing temperatures.

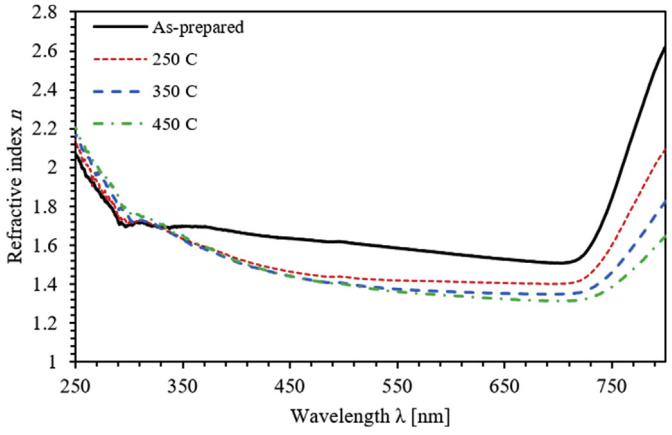

Figure 13. The Refractive index of CZTS thin films at different annealing temperatures.

Table 1. The calculated elastic constants (C_{ij}), bulk modulus (K), shear modulus (G), Young's modulus (E), and Poisson's ratio (ν) of the CZTS thin films.

Parameter	This work	Ref. [71]
C_{11} (GPa)	91.61	91.61
C_{12} (GPa)	57.38	57.40
C_{13} (GPa)	55.42	55.40
C_{33} (GPa)	91.80	91.54
C_{44} (GPa)	40.40	40.32
C_{44} (GPa)	42.21	42.18
K_V (GPa)	67.74	67.91
K_R (GPa)	67.74	67.90
K_{VRH} (GPa)	67.74	67.90
G_V (GPa)	31.63	31.67
G_R (GPa)	26.69	26.87
G_{VRH} (GPa)	29.16	29.27
E (GPa)	76.50	76.78
ν	0.312	0.312
K/G	2.32	2.32

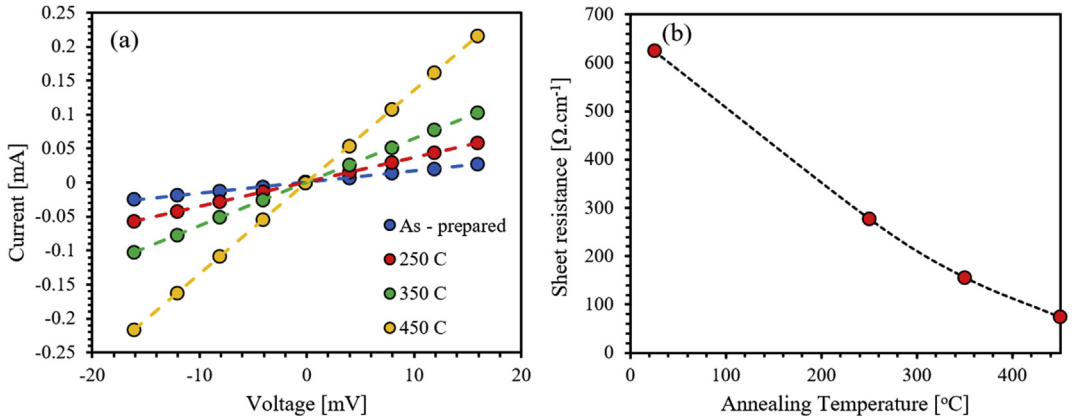

Figure 14. (a) The I–V plot of CZTS thin films at various annealing temperatures, (b) Sheet resistance of CZTS thin films as a function of annealing temperature.

4. Summary and conclusion

In summary, the CZTS thin films are prepared using the sol-gel method and deposited on glass substrates by immersing method. The effect of annealing temperature on structural, chemical, optical, electrical, and elastic properties of CZTS thin films is investigated. The XRD analysis showed that CZTS thin films annealed at 450 °C exhibit a kesterite structure to the tetragonal system. SEM micrographs reveal that as-prepared CZTS thin film is amorphous and exhibits a polished smooth surface. However, annealed CZTS thin films appear to consist of spherical particles that become more apparent and more crystallized at 450 °C annealing temperature indicating a drastic surface morphological change upon annealing. The optical parameters of annealed CZTS thin films compared to those of as-prepared thin films. In particular, a remarkable decrease of the optical band gap energy to 1.6 eV is observed for thin films annealed at 450°. The observed significant change of the absorption coefficient of annealed CZTS thin films may be explained in terms of the increase of the crystalline size and crystallinity in agreement with XRD results. From the mechanical point of view, as the annealing temperature increases, the crystallite size increases, and the microstrain decreases. The drastic changes of these two parameters result in enhancing the photovoltaic performance of CZTS thin films based solar cells.

Furthermore, sheet resistance exhibits a significant decrease from 625 $\Omega.cm^{-1}$ to 74 $\Omega.cm^{-1}$ as the annealing temperature is increased. Such a remarkable reduction of the sheet resistance has important implications for implementing CZTS thin films in several optoelectronic applications. Additionally, modulating the sheet resistance drastically by increasing the annealing temperature would significantly affect the electrical properties of thin films. The bulk modulus of CZTS is obtained to be 67.74 GPa. Strikingly, Poisson's ratio is estimated to be about 0.3, indicating that CZTS has good plasticity. In the contest of the results of this work, multifunctional and multi-junctional CZTS scaled thin film-based solar cells of remarkable electrical properties, mechanically stable, and extraordinary optical properties may be fabricated commercially.

Declarations

Author contribution statement

Ahmad A. Ahmad, Ahmad B. Migdadi, Ahmad M. Alsaad, I. A. Qattan, Qais M. Al-Bataineh, Ahmad Telfah: conceived and designed the experiments; performed the experiments; analyzed and interpreted the data; contributed reagents, materials, analysis tools or data; wrote the paper.

Funding statement

This work was supported by the Faculty of Scientific Research faculty at Jordan University of Science and Technology (JUST) (350–2020).

Data availability statement

Data will be made available on request.

Declaration of interests statement

The authors declare no conflict of interest.

Additional information

No additional information is available for this paper.

Acknowledgements

The authors would like to thank Prof. Borhan Albiss and Prof. M-Ali Al-Akhras for their help using the Center of Nanotechnology and the Lab of Biomedical Physics.

References

[1] M. Suryawanshi, et al., CZTS based thin film solar cells: a status review, Mater. Technol. 28 (1-2) (2013) 98–109.
[2] P. Jackson, et al., New world record efficiency for Cu (In, Ga) Se2 thin-film solar cells beyond 20%, Prog. Photovolt. Res. Appl. 19 (7) (2011) 894–897.
[3] S. Zhuk, et al., Molybdenum Incorporated Cu1. 69ZnSnS4 Kesterite Photovoltaic Devices with Bilayer Microstructure and Tunable Optical-Electronic Properties, Sol. Energy 194 (2019) 777–787.
[4] T.H. Nguyen, et al., Cu 2 ZnSnS 4 thin film solar cells with 5.8% conversion efficiency obtained by a facile spray pyrolysis technique, RSC Adv. 5 (95) (2015) 77565–77571.
[5] A. Moholkar, et al., Studies of compositional dependent CZTS thin film solar cells by pulsed laser deposition technique: an attempt to improve the efficiency, J. Alloys Compd. 544 (2012) 145–151.
[6] K. Ito, T. Nakazawa, Electrical and optical properties of stannite-type quaternary semiconductor thin films, Jpn. J. Appl. Phys. 27 (11R) (1988) 2094.
[7] N. Kamoun, H. Bouzouita, B. Rezig, Fabrication and characterization of Cu2ZnSnS4 thin films deposited by spray pyrolysis technique, Thin Solid Films 515 (15) (2007) 5949–5952.
[8] S. Chen, et al., Intrinsic point Defects and Complexes in the Quaternary Kesterite Semiconductor Cu 2 ZnSnS 4 81, 2010, p. 245204 (24).
[9] W. Wang, et al., Device characteristics of CZTSSe thin-film solar cells with 12.6% efficiency, Adv. Energy Mater. 4 (7) (2014) 1301465.
[10] W. Shockley, H.J. Queisser, Detailed balance limit of efficiency of p-n junction solar cells, J. Appl. Phys. 32 (3) (1961) 510–519.
[11] S. Pawar, et al., Single Step Electrosynthesis of Cu2ZnSnS4 (CZTS) Thin Films for Solar Cell Application 55, 2010, pp. 4057–4061 (12).
[12] N. Khoshsirat, et al., Efficiency Enhancement of Cu2ZnSnS4 Thin Film Solar Cells by Chromium Doping 201, 2019, p. 110057.
[13] C. Yan, et al., Cu 2 ZnSnS 4 Solar Cells with over 10% Power Conversion Efficiency Enabled by Heterojunction Heat Treatment 3, 2018, pp. 764–772 (9).
[14] W. Wang, et al., Device Characteristics of CZTSSe Thin-Film Solar Cells with 12.6% Efficiency 4, 2014, p. 1301465 (7).
[15] B. Shin, et al., Thin Film Solar Cell with 8.4% Power Conversion Efficiency Using an Earth-Abundant Cu2ZnSnS4 Absorber 21, 2013, pp. 72–76 (1).
[16] I. Repins, et al., Co-evaporated Cu2ZnSnSe4 Films and Devices 101, 2012, pp. 154–159.

[17] P. Fernandes, P. Salomé, A. Da Cunha, Growth and Raman scattering characterization of Cu2ZnSnS4 thin films, Thin Solid Films 517 (7) (2009) 2519–2523.
[18] S. Schorr, Structural aspects of adamantine like multinary chalcogenides, Thin Solid Films 515 (15) (2007) 5985–5991.
[19] S. Vanalakar, et al., A Review on Pulsed Laser Deposited CZTS Thin Films for Solar Cell Applications 619, 2015, pp. 109–121.
[20] L. Peng, et al., Effect of Annealing Temperature on the Structure and Optical Properties of In-Doped ZnO Thin Films 484, 2009, pp. 575–579 (1-2).
[21] Y. Zhao, et al., Structural and Elastic DFT Study of Four Structures for Cu2ZnSnS4 under High Pressure 696, 2017, pp. 86–95.
[22] I. Camps, et al., Elastic and Optical Properties of Cu2ZnSn (SexS1− x) 4 Alloys: Density Functional Calculations 27, 2012, p. 115001 (11).
[23] A. Weber, et al., Multi-stage Evaporation of Cu2ZnSnS4 Thin Films 517, 2009, pp. 2524–2526 (7).
[24] J.-S. Seol, et al., Electrical and Optical Properties of Cu2ZnSnS4 Thin Films Prepared by Rf Magnetron Sputtering Process 75, 2003, pp. 155–162 (1-2).
[25] C. Chan, et al., Preparation of Cu2ZnSnS4 Films by Electrodeposition Using Ionic Liquids 94, 2010, pp. 207–211 (2).
[26] H. Yoo, J. Kim, S. Cells, Comparative study of Cu2ZnSnS4 film growth, Sol. Energy Mater. Sol. Cell. 95 (1) (2011) 239–244.
[27] L. Sun, et al., Structure, Composition and Optical Properties of Cu2ZnSnS4 Thin Films Deposited by Pulsed Laser Deposition Method 95, 2011, pp. 2907–2913 (10).
[28] J. Hafner, Ab-initio simulations of materials using VASP: density-functional theory and beyond, J. Comput. Chem. 29 (13) (2008) 2044–2078.
[29] P. Hohenberg, W. Kohn, Inhomogeneous electron gas, Phys. Rev. 1964 (136) (1964) B864.
[30] W. Kohn, L.J. Sham, Self-consistent equations including exchange and correlation effects, Phys. Rev. 1965 (140) (1965) A1133.
[31] G. Kresse, D. Joubert, From ultrasoft pseudopotentials to the projector augmented-wave method, Phys. Rev. 1999 (59) (1999) 1758, 1758.
[32] B. Adolph, J. Furthmüller, F. Bechstedt, Optical properties of semiconductors using projector-augmented waves, Phys. Rev. B 63 (12) (2001) 125108.
[33] P.E. Blöchl, Projector augmented-wave method, Phys. Rev. B 50 (24) (1994) 17953.
[34] G. Kresse, J. Hafner, Ab initio molecular-dynamics simulation of the liquid-metal–amorphous-semiconductor transition in germanium, Phys. Rev. B 49 (20) (1994) 14251.
[35] S. Bates, G. Kresse, M. Gillan, A systematic study of the surface energetics and structure of TiO2(110) by first-principles calculations. Surface Science 385 (2-3) (1997) 386–394.
[36] G. Kresse, G. Kresse, J. Furthmüller, Efficient iterative schemes for *ab initio* total-energy calculations using a plane-wave basis set, Phys. Rev. B 1996 (54) (1996) 11169.
[37] J. Wang, et al., Oxygen vacancy induced band-gap narrowing and enhanced visible light photocatalytic activity of ZnO, ACS Appl. Mater. Interfaces 4 (8) (2012) 4024–4030.
[38] A. Kohan, et al., First-principles study of native point defects in ZnO, Phys. Rev. B 61 (22) (2000) 15019.
[39] S. Vanalakar, et al., Effect of post-annealing Atmosphere on the Grain-Size and Surface Morphological Properties of Pulsed Laser Deposited CZTS Thin Films 40, 2014, pp. 15097–15103 (9).
[40] A. Khalkar, et al., Effect of Growth Parameters and Annealing Atmosphere on the Properties of Cu2ZnSnS4 Thin Films Deposited by Cosputtering, 2013, p. 2013.
[41] Y.K. Kumar, et al., Preparation and Characterization of spray-deposited Cu2ZnSnS4 Thin Films 93, 2009, pp. 1230–1237 (8).
[42] A. Weber, et al., In-situ XRD on Formation Reactions of Cu2ZnSnS4 Thin Films 6, 2009, pp. 1245–1248 (5).
[43] Ziaeifar, F., et al., Synthesis of Cu2S film by SILAR, spray pyrolysis and Zn-Cu alloy methods.
[44] Q.M. Al-Bataineh, et al., Synthesis, crystallography, microstructure, crystal defects, optical and optoelectronic properties of ZnO: CeO2 mixed oxide thin films, in: Photonics, Multidisciplinary Digital Publishing Institute, 2020.
[45] T. Özdal, et al., Effect of Annealing Temperature on Morphology and Optoelectronics Properties of Spin-Coated CZTS Thin Films, 2020, pp. 1–11.
[46] S. Kose, et al., Some Physical Properties of Copper Oxide Films: the Effect of Substrate Temperature 111, 2008, pp. 351–358 (2-3).
[47] S. Kurtaran, Al doped ZnO thin films obtained by spray pyrolysis technique: influence of different annealing time, Opt. Mater. 114 (2021) 110908.
[48] H. Faiz, et al., Effect of Zinc Induced Compressive Stresses on Different Properties of Copper Oxide Thin Films 89, 2015, pp. 353–360 (4).
[49] S. Adachi, Earth-abundant Materials for Solar Cells: Cu2-II-IV-VI4 Semiconductors, John Wiley & Sons, 2015.
[50] Z.A. Tsegaye, Density Functional Theory Studies of Electronic and Optical Properties of ZnS Alloyed with Mn and Cr, Institutt for fysikk, 2012.
[51] Q.M. Al-Bataineh, et al., Structural, electronic and optical characterization of ZnO thin film-seeded platforms for ZnO nanostructures: sol–gel method versus ab initio calculations, J. Electron. Mater. 48 (8) (2019) 5028–5038.
[52] G. Qin, et al., First-principles investigation of the electronic and magnetic properties of ZnO nanosheet with intrinsic defects, Comput. Mater. Sci. 81 (2014) 259–263.
[53] K. Li, et al., Ferromagnetism in phosphorus-doped ZnO: first-principles calculation, Phys. Lett. 374 (4) (2010) 628–631.
[54] D.K. Maurya, et al., Synthesis and characterization of nanostructured copper zinc tin sulphide (CZTS) for humidity sensing applications, IEEE Sensor. J. 19 (8) (2019) 2837–2846.
[55] R. Mainz, et al., Real-time observation of Cu 2 ZnSn (S, Se) 4 solar cell absorber layer formation from nanoparticle precursors, Phys. Chem. Chem. Phys. 15 (41) (2013) 18281–18289.
[56] E. Indubala, et al., Non-vacuum synthesis of CZTS by sulphurization of electrochemically layered zinc and tin on copper, Mater. Sci. Semicond. Process. 101 (2019) 37–45.
[57] M. Dahnoun, et al., Structural, optical and electrical properties of zinc oxide thin films deposited by sol-gel spin coating technique, Optik 134 (2017) 53–59.
[58] A. Ahmad, et al., Optical and Structural Investigations of Dip-Synthesized boron-doped ZnO-Seeded Platforms for ZnO Nanostructures 124, 2018, pp. 1–13 (6).
[59] Y. Zhang, et al., Effect of Annealing Temperature on the Structural and Optical Properties of ZnO Thin Films Prepared by Sol–Gel Method 16, 2010, pp. 815–820 (9).
[60] M. Arif, et al., Effect of Annealing Temperature on Structural and Optical Properties of Sol-Gel-Derived ZnO Thin Films 47, 2018 (7).
[61] M. Byeon, et al., The Effects for the Deposition Temperature onto the Structural, Compositional and Optical Properties of Pulsed Laser Ablated Cu2ZnSnS4 Thin Films Grown on Soda Lime Glass Substrates 546, 2013, pp. 387–392.
[62] A. Alsaad, et al., Optical Band gap and Refractive index Dispersion Parameters of boron-doped ZnO Thin Films: A Novel Derived Mathematical Model from the Experimental Transmission Spectra 211, 2020, p. 164641.
[63] A.Y. Fasasi, et al., Effect of Precursor Solvents on the Optical Properties of Copper Oxide Thin Films Deposited Using spray Pyrolysis for Optoelectronic Applications 3, 2018, p. 12.
[64] A.S. Hassanien, A.A. Akl, Influence of composition on optical and dispersion parameters of thermally evaporated non-crystalline Cd50S50− xSex thin films, J. Alloys Compd. 648 (2015) 280–290.
[65] S.G. Lee, et al., Structural, Morphological, Compositional, and Optical Properties of Single Step Electrodeposited Cu2ZnSnS4 (CZTS) Thin Films for Solar Cell Application 14, 2014, pp. 254–258 (3).
[66] Q.M. Al-Bataineh, et al., Structural, Electronic and Optical Characterization of ZnO Thin Film-Seeded Platforms for ZnO Nanostructures: Sol–Gel Method versus Ab Initio Calculations 48, 2019, pp. 5028–5038 (8).
[67] R. Gaillac, P. Pullumbi, F.-X. Coudert, ELATE: an open-source online application for analysis and visualization of elastic tensors, J. Phys. Condens. Matter 28 (27) (2016) 275201.
[68] Z. Huang, et al., Electronic Structural, Elastic Properties and Thermodynamics of Mg17Al12, Mg2Si and Al2Y Phases from First-Principles Calculations 407, 2012, pp. 1075–1081 (7).
[69] Y.F. Zhao, Z.M. Liu, D.C. Li, Theoretical study of structural, elastic properties and phase transitions of Cu2ZnSnS4, in: Advanced Materials Research, Trans Tech Publ, 2014.
[70] S. Pugh, XCII. Relations between the Elastic Moduli and the Plastic Properties of Polycrystalline Pure Metals. The London, Edinburgh, and Dublin Philosophical Magazine and Journal of Science 45, 1954, pp. 823–843 (367).
[71] X. He, et al., Elastic and thermo-physical properties of stannite-type Cu 2 ZnSnS 4 and Cu 2 ZnSnSe 4 from first-principles calculations, Acta Metall. Sin. 26 (3) (2013) 285–292.